Karaelmas Science and Engineering Journal

Journal home page: https://dergipark.org.tr/tr/pub/karaelmasfen DOI: 10.7212/karaelmasfen.1752771

Research Article

Received / Geliş tarihi : 28.07.2025 Accepted / Kabul tarihi : 22.08.2025



Evaluation of the Radiation Shielding Properties of Hydrothermally Synthesized CuO Nanoparticles via Monte Carlo FLUKA Simulations

Monte Carlo FLUKA Simülasyonları Kullanılarak Hidrotermal Olarak Sentezlenen CuO Nanopartiküllerinin Radyasyon Kalkanı Özelliklerinin Değerlendirilmesi

Saniye Tekerek* ®

Kahramanmaraş Sütçü İmam University, Vocational School of Health Services, Department of Medical Services and Techniques, Kahramanmaraş, Türkiye

Abstract

Copper oxide nanoparticles (CuO NPs) were synthesized at 105 °C via a hydrothermal deposition technique. The structure of the CuO nanoparticles was characterized via X-ray diffraction (XRD), and morphological analysis was performed by scanning electron microscopy (SEM). The optical properties of the nanoparticles were examined via a UV-vis spectrophotometer. X-ray diffraction analysis revealed the monoclinic phase. The direct optical bandwidth of the nanoparticles was found to be 2.88 eV. On the basis of optical measurements, optical parameters such as the refractive index (n), extinction coefficient (k), and real (£1) and imaginary (£2) components of the dielectric constant were calculated. At a wavelength of 550 nm, the optical constants n and k were found to be 2.75 and 0.00024, respectively, corresponding to dielectric real and imaginary constants of 7.570 and 0.0013. Additionally, photon interactions with CuO NPs at various energy levels were simulated via the FLUKA program. The energy deposition in the material provided valuable information for assessing the radiation shielding capabilities of the investigated material.

Keywords: CuO nanoparticles, FLUKA simulation, Monte Carlo, optical parameters, radiation shielding.

Öz

Bakır oksit nanoparçacıkları (CuO NP), 105 °C'de hidrotermal depolama yöntemiyle sentezlendi. CuO nanopartiküllerinin yapısal analizi X-ışını kırınımı (XRD) ile karakterize edildi ve morfolojik analizi taramalı elektron mikroskobu (SEM) ile gerçekleştirildi. Optik özellikleri ise UV-vis spektrofotometersi kullanılarak incelendi. X-ışını kırınımı analizi monoklinik fazı ortaya çıkardı. Nanopartiküllerin direkt optik bant genişliği 2,88 eV olarak bulundu. Optik ölçümlere dayanarak kırılma indisi (n), soğurma katsayısı (k) ve dielektrik sabitinin gerçek (ε1) ve sanal (ε2) bileşenleri gibi optik parametreler hesaplandı. 550 nm dalga boyunda, n ve k değerleri sırasıyla 2,75 ve 0,00024 olarak bulunurken, bu değerlere karşılık gelen gerçek ve sanal dielektrik sabitlerinin değerleri 7,570 ve 0,0013 olarak bulundu. Ayrıca, farklı enerji seviyelerinde fotonların CuO NP'lerle etkileşimi FLUKA programı ile simüle edildi. Malzemedeki enerji birikimi, çalışılan malzemenin radyasyon zırhlama özelliklerini değerlendirmek için önemli bilgiler sağladı.

Anahtar Kelimeler: CuO nanopartikülleri, FLUKA simülasyonu, Monte Carlo, optik parametreler, radyasyon kalkanı.

1. Introduction

The attenuation of radiation has been employed as a valuable tool in scientific studies, medicine, and agriculture. Although such applications are highly advantageous to human life, unintended exposures such as cosmic rays and scattering

the risk of cancer and can have negative effects (Mullenders 2009, Meulepas et al. 2018). Protective substances are used to block radiation from a variety of sources, including nuclear waste treatment facilities, laboratories, and X-ray rooms. Recent studies have investigated the radiation shielding and attenuation properties of various glass systems, metal oxides, ferrite nanostructures, and metallic alloys. Recent reports indicate the utilization of Pb-Se alloys (Mansy et al. 2021)

and the gamma-ray shielding capabilities of Al₂O₃/PbO₂ nanoparticles (Ali et al. 2020). Researchers have investi-

gamma rays pose a threat to people and their surroundings in a variety of ways. High gamma-dose exposure can increase

*Corresponding author: saniyetekerek@ksu.edu.tr Saniye Tekerek © orcid.org/0000-0003-3326-358X



gated the radiation shielding of Na₂O–P₂O₅ glasses doped with MnO via FLUKA and Phy-X, studied nanoscale metal oxides, and analyzed radiation attenuation via Monte Carlo simulations (Dridi et al. 2024). They used FLUKA to study γ-ray attenuation in metals, alloys, and metal oxides. They also evaluated nuclear radiation attenuation in binary nanocomposites (El-Taher et al. 2025), investigated the shielding performance of tellurite glasses with Li₂O and MoO₃ using XCOM and FLUKA (Alzahrani et al. 2024), and simulated the shielding parameters of Gd–Pb alloys with FLUKA and Phy-X/PSD (Rehman et al. 2025). However, despite this extensive research, no study has specifically examined the radiation storage and absorption of CuO metal oxide nanoparticles. This gap highlights the novelty and importance of the present work.

This study aims to investigate the effect of material thickness on the radiation shielding performance of CuO NPs produced via the hydrothermal method. Owing to its high atomic number and density, CuO is a promising candidate for radiation shielding materials. To determine the radiation shielding properties of the current CuO nanoparticles, the FLUKA simulation program was used. The FLUKA code is extensive simulation software that covers various applications, including radiation physics (Ferrari et al. 2005). This study is critical for advancing the use of CuO NPs in fields requiring efficient radiation shielding, such as medical imaging and nuclear technology.

2. Materials and Methods

2.1. Synthesis of CuO Nanoparticles

CuO nanoparticles were obtained via a hydrothermal method with a 0.2 M copper(II) acetate monohydrate precursor solution. The Cu precursor solution was mixed in 75 ml of distilled water for 15 min at 50 °C. Simultaneously, a 0.4 M NaOH pellet was added and stirred in 25 mL of distilled water, after which the resulting solution was slowly added to the CuO precursor solution. At the end of this process, a homogeneous dark blue solution was obtained. The final solution was stirred for 30 min at 50 °C and then for 30 min at room temperature. The solution, which was measured at pH 9.5, was placed in Teflon and then in an autoclave container and kept in a muffle furnace at 105 °C for 12 hours. Finally, the recrystallized powder was filtered, and the product powders were cleaned with distilled water three times and then air dried. As a result, the CuO nanostructures obtained via the hydrothermal method were lightweight, nanoscale in size, and black in color.

2.2. Characterization

The structure and lattice parameters of the CuO NPs were obtained via X-ray diffraction (XRD) (Scintag XDS2000) with Cu K α radiation (λ = 0.154 nm) in the range of 10–80°. The surface properties of the present nanoparticles were revealed by scanning electron microscopy (SEM) (model FEI Quanta 250 FEG). Finally, optical transmittance measurements were carried out in the wavelength range from 400–1100 nm with a UV/visible spectrophotometer (Shimadzu UV-2600).

2.3. Radiation Attenuation Performance

This study was conducted to determine the optimum radiation attenuation parameters for the synthesized CuO NPs. In the context of this study, FLUKA was used to simulate the interactions of photons with CuO NPs at different energy levels. Theoretical data were obtained via the FLUKA code, a comprehensive simulation software that covers various applications, including radiation physics (Ferrari et al. 2005, Ballarini et al. 2006). FLUKA refers to the fully integrated Monte Carlo simulation software package developed since 1989. It includes the FLUKA core code and the Flair user interface. FLUKA is a general-purpose tool for calculating particle transport and interactions with matter, covering a wide range of applications, from proton and electron accelerator shielding to target design, calorimetry, activation, dosimetry, detector design, particle accelerators, cosmic rays, neutrino physics, and radiotherapy. The FLU-KA program calculates the energy deposition and particle flux in the material, providing valuable information for assessing the radiation shielding and energy storage capabilities of the material under investigation. FLUKA is a comprehensive Monte Carlo simulation code that models complex radiation transport and interactions in 3D geometries, including secondary particle production and energy deposition. The simulation allows for the determination of the radiation absorption efficiency, energy deposition profiles, and overall performance of the NPs under various irradiation conditions. The results are essential for evaluating the effectiveness of the NPs as radiation shields and their suitability for use in applications where radiation exposure is a concern. WinXCom, the Windows-based version of the NIST XCOM database (Hubbell 1969), is widely used for calculating photon interaction parameters such as the mass attenuation coefficient, effective atomic number, and electron density over a broad energy range (1 keV-100 GeV). This allows researchers to define custom materials by their elemental compositions, making them ideal for studying the

radiation shielding properties of various substances. Owing to its accuracy and ease of use, WinXCom is frequently employed in combination with Monte Carlo simulation tools such as FLUKA for validation and comparative analysis in shielding studies. WinXCom and Phy-X/PSD are analytical tools for calculating photon interaction parameters such as mass attenuation coefficients, effective atomic numbers, and electron density. While FLUKA delivers high-precision, geometry-specific results, it demands greater computational resources and expertise. Therefore, WinXCom and Phy-X/PSD are preferred for rapid analytical calculations, whereas FLUKA is better suited for detailed simulation

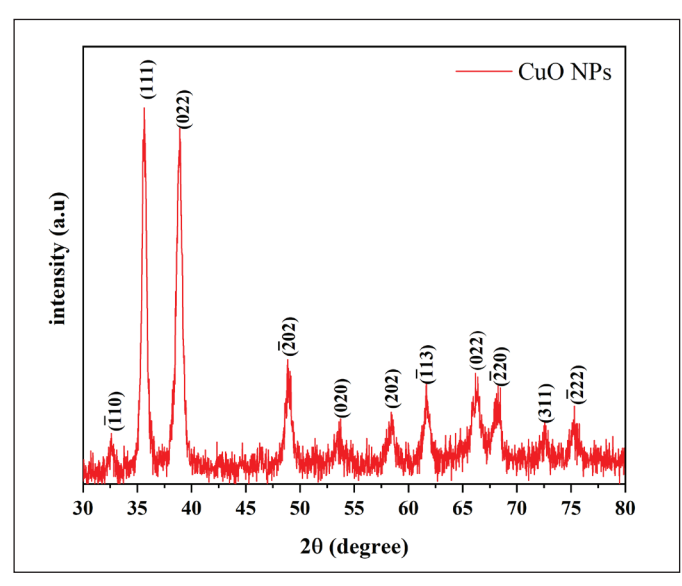


Figure 1. XRD pattern of CuO NPs produced by the hydrothermal method.

studies (Hubbell and Seltzer 2004, Ballarini et al. 2006, Şakar et al. 2020).

3. Results and Discussion

3.1. Structural Analysis

The structural properties of the CuO NPs were analyzed via X-ray diffraction (XRD). Figure 1 shows the crystalline structure of CuO NPs synthesized via the hydrothermal method. The diffraction peaks corresponding to the monoclinic phase structure of CuO are located in Table 1. The CuO NPs are well indexed to a monoclinic crystalline nature (a= 4.68 Å, b= 3.42 Å, c= 5.13, a/b= 1.37, c/b= 1.50 Å; density= 6.52 g/cm³; volume= 81.08 cm³). The sharp and strong peaks are assumed to be due to the cubic crystal structures of the CuO phase (Basith et al. 2013, Nandhakumar et al. 2019, Amri et al. 2019).

The crystal size of the nanoparticles was calculated via the Debye–Scherrer formula (Equation 1). For the CuO NPs, the Debye–Scherrer relationship was used to calculate the crystallite size () (Stokes and Wilson 1944):

$$D = \frac{0.9\lambda}{\beta\cos\theta} \tag{1}$$

where λ is the X-ray wavelength (0.15406 nm for Cu K α), θ is Bragg's diffraction angle, and β is the peak's full width at half maximum (FWHM) in radians. For the observed diffraction peaks, the crystallite sizes were calculated and are given in Table 2. Using the Debye–Scherrer Equation (1), the average crystal size of the obtained CuO NPs was calculated to be approximately 11.68 nm.

Table 1	Structural	narameters	$\circ f$	C_{11}	NP_{c}
Table L.	энисппа	Darameters	()		INFS

Material	Observed values		Sta	Standard values		JCPDS card	Phase
	2θ (°)	d (Å)	2θ (°)	d (Å)	(hkl)	no	Filase
	32.62	2.75	32.53	2.74	(-110)	01-073-6023	Monoclinic (CuO)
	35.63	2.52	35.55	2.52	(111)	01-073-6023	Monoclinic (CuO)
	38.91	2.31	38.92	2.30	(022)	01-073-6023	Monoclinic (CuO)
48.88 53.73 CuO NPs 58.39 61.66 66.19 68.23	1.86	48.75	1.85	(-202)	01-073-6023	Monoclinic (CuO)	
	1.71	53.50	1.70	(020)	01-073-6023	Monoclinic (CuO)	
	58.39	1.58	58.35	1.57	(202)	01-073-6023	Monoclinic (CuO)
	61.66	1.50	61.57	1.50	(-113)	01-073-6023	Monoclinic (CuO)
	66.19	1.40	65.84	1.42	(022)	01-073-6023	Monoclinic (CuO)
	68.23	1.37	68.14	1.37	(-220)	01-073-6023	Monoclinic (CuO)
	72.55	1.30	72.42	1.30	(311)	01-073-6023	Monoclinic (CuO)
	75.31	1.26	75.82	1.26	(-222)	01-073-6023	Monoclinic (CuO)

Table 2.	The cr	vstallite	sizes	of	CuO	NPs.
----------	--------	-----------	-------	----	-----	------

2θ (°)	d (Å)	FWHM	Cristal size (nm)
32.62	2.75	0.57531	14.38
35.63	2.52	0.57074	14.62
38.91	2.31	0.70486	11.95
48.88	1.86	0.71366	12.23
53.73	1.71	0.76695	11.61
58.39	1.58	0.64679	14.07
61.66	1.50	0.63047	14.67
66.19	1.40	1.05725	8.969
68.23	1.37	0.80599	11.91
72.55	1.30	340.9137	0.029
75.31	1.26	0.71442	14.04

3.2. Morphological Analysis

SEM was used to analyze the surface morphology of the synthesized CuO NPs. Figure 2 shows SEM images of the produced nanoparticles at different magnifications. As shown in this figure, the nanoparticles exhibited a flower-like morphology. A similar morphology for CuO nanoparticles was reported in previous work (Rai 2024). According to the SEM images and surface morphology of the CuO NPs, constructed from agglomerated nanoparticles in the range of 40–90 nm, formed a mesoporous surface.

3.3. Optical Properties

The optical properties of the CuO NPs were determined via absorbance measurements conducted at room temperature. The optical absorbance spectrum is crucial for assessing a material's optical properties. The optical absorbance and transmittance spectra of the nanoparticles are shown in Figures 3(a) and (b), respectively. In the visible range (λ = 550 nm), the absorption spectrum of the CuO NPs decreased, whereas the transmittance exhibited the opposite trend.

The nanoparticle absorbance coefficient (α) was determined via the following relation (Perkowitz 1993):

$$T = e^{-\alpha t} \tag{2}$$

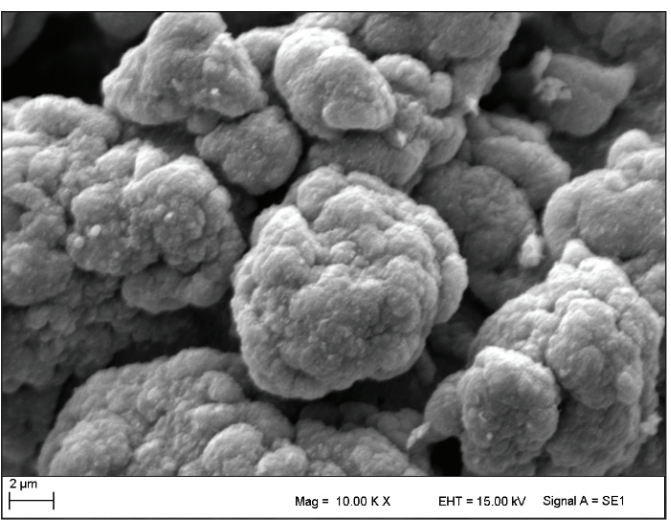
where t is the thickness, and where T is the transmittance. The reflection spectra (R) of the nanoparticles shown in Figure 3(b) were calculated via Equation 3.

$$T = (1 - R)^2 \exp(-A) \tag{3}$$

where R is the reflectance. At $\lambda = 550$ nm, the reclectance of the nanoparticles exhibited a similar behavior as the absorption.

The absorbance of the CuO NPs produced by the hydrothermal method is shown in Figure 3a, and the transmittance and reflectance changes are shown in Figure 3b. This also indicates that the CuO NPs significantly absorbed incident photons over a wide range of solar wavelengths, with absorption edges observed at 500–650 nm. The CuO NPs, which have 26.31% transmittance at 300 nm in the UV region, have 85.65% transmittance in the visible region between 400 and 600 nm. These behaviors can be explained by the high transmittance (> 26% in the UV region of CuO), as illustrated in Figure 3b; for longer wavelengths (> 380 nm), they become transparent.

The optical band width (E_g) values of the CuO NPs were calculated by extrapolating a linear relationship between the $(\alpha h v)^2$ and photon energy (h v) curves to the energy axis when $(\alpha h v)^2 = 0$, as shown in Figure 4. The variation in α



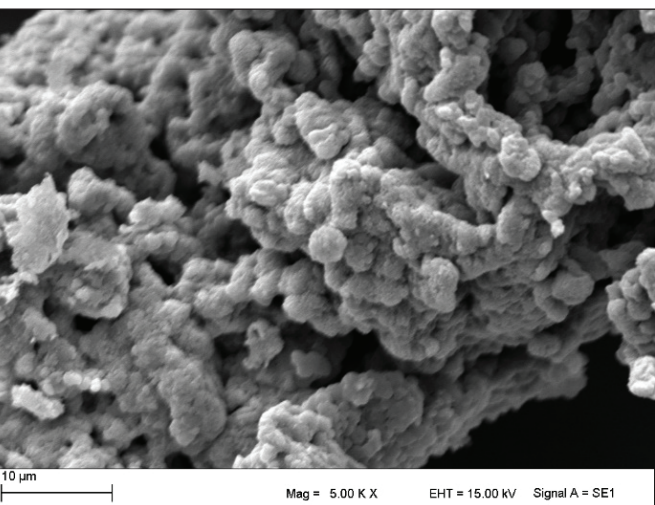


Figure 2. SEM images of CuO NPs at different magnifications.

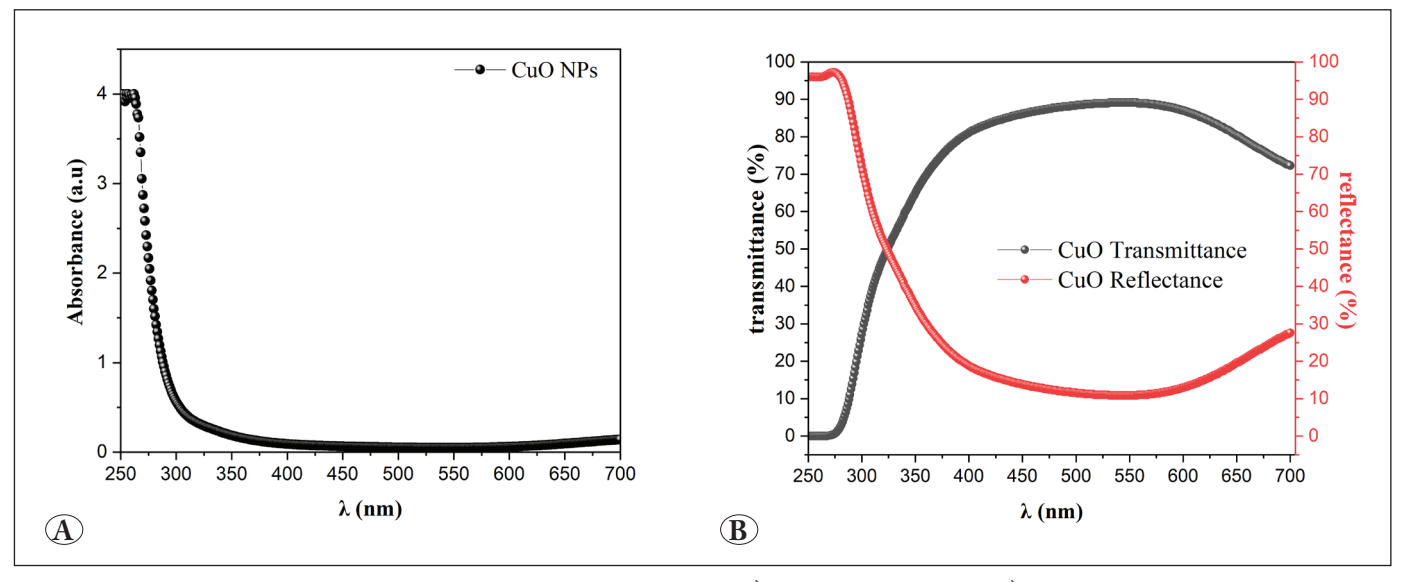


Figure 3. The CuO NPs produced via the hydrothermal method **A)** the absorbance and **B)** the transmittance and reflectance changes graph.

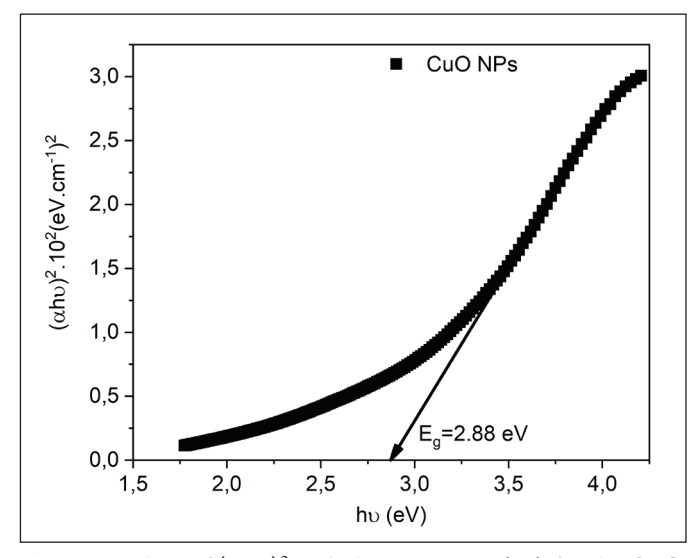


Figure 4. Plots of $(\alpha hv)^2$ and photon energy (hv) for the CuO NPs.

with *hv* is given by the power law of Tauc's relation (Tauc 1974):

$$(\alpha h v) = C(h v - E_v)^n \tag{4}$$

where C is a constant, hv is the incident photon energy, and n represents the transition type. For an allowed direct transition, n is equal to $\frac{1}{2}$, whereas for an allowed indirect transition, n is equal to 2. The Tauc plot of the UV-vis data collected in the wavelength range of 250–700 nm, shown in Figure 4, was used to calculate the optical band gap of the CuO NPs. The energy band gap calculated from the plot of

(αhv)² as a function of photon energy (hv) was found to be 2.88 eV. The present band gap widths of the CuO NPs are in excellent agreement with the values reported in previous studies (Sagadevan et al. 2017, Chen et al. 2018, Nitta et al. 2022).

Optical parameters such as the refractive index (n), extinction coefficient (k), reel (ϵ_1) , and imaginary (ϵ_2) parts of the complex dielectric constant can be calculated via UV-vis spectra via the following relationships (Wooten 1972, Moss et al. 1973).

$$k = \frac{\alpha \lambda}{4\pi} \tag{5}$$

$$n = \frac{1+R}{1-R} + \sqrt{\frac{4R}{(1-R)^2} - k^2}$$
 (6)

$$\varepsilon_1 = n^2 + k^2 \tag{7}$$

$$\varepsilon_2 = 2nk \tag{8}$$

The plots of n and k as a function of wavelength are shown in Figures 5(a) and (b), respectively. At a wavelength of 550 nm, the n value was 2.75, whereas the k value was 0.00024 (Table 3). The variations in the ε_1 and ε_2 values with respect to the wavelength are shown in Figures 5(c) and (d), respectively. As seen from these graphs and Table 3, the ε_1 value is 7.570, whereas the ε_2 value is 0.0013.

3.4. Radiation Shielding Performance

Figure 6 presents the FLUKA-based simulation setup designed to replicate the experimental conditions for

Table 3. Optical parameters of CuO NPs at 550 nm.

Material	E_{g} (eV)	λ=550 nm					
		n	k	$\epsilon_{_1}$	ϵ_2		
CuO NPs	2.88	2.75	0.00024	7.570	0.0013		

evaluating photon attenuation in the target sample. The plot of the variation in the HVL values with energy, expressed as the layer thickness (cm) that can absorb half of the amount of radiation interacting with the material, is given in Figure 7. The half value layer (HVL) and tenth value layer (TVL) are the required thicknesses to reduce the high photon intensities by one half and one tenth, respectively (Agar et al. 2019). Moreover, the mean free path (MFP), which indicates the average distance that radiation travels in the material before interacting, is inversely related to the linear attenuation coefficient (μ) (Sayyed et al. 2018). The mass attenuation coefficient (μ / ρ) is used to obtain these parameters as follows:

$$HVL = \frac{In\left(\frac{100}{50}\right)}{\mu} = \frac{In2}{\mu} \tag{9}$$

$$TVL = \frac{In\left(\frac{100}{10}\right)}{\mu} = \frac{In10}{\mu} \tag{10}$$

$$MFP = \frac{1}{\mu} \tag{11}$$

For the CuO NPs examined, a low HVL value means that the material interaction with radiation is greater, and at 100 keV, energy absorbs more radiation. It was found to have an HVL value of 0.27 cm at 100 keV (Figure 7). The highest HVL thickness value was obtained for the 1.83 cm CuO NPs at an energy of 1 MeV. The variation graph of the tenth value layer for the layer thickness, which can absorb 1/10 of the radiation interacting with the material as a function of energy, is shown in Figure 7. The TVL value increased to 10 MeV, after which it gradually decreased until 20 MeV. The CuO NPs had the highest mean free path (MFP) value, approximately 5.4 cm, at an energy of 900 keV. For CuO

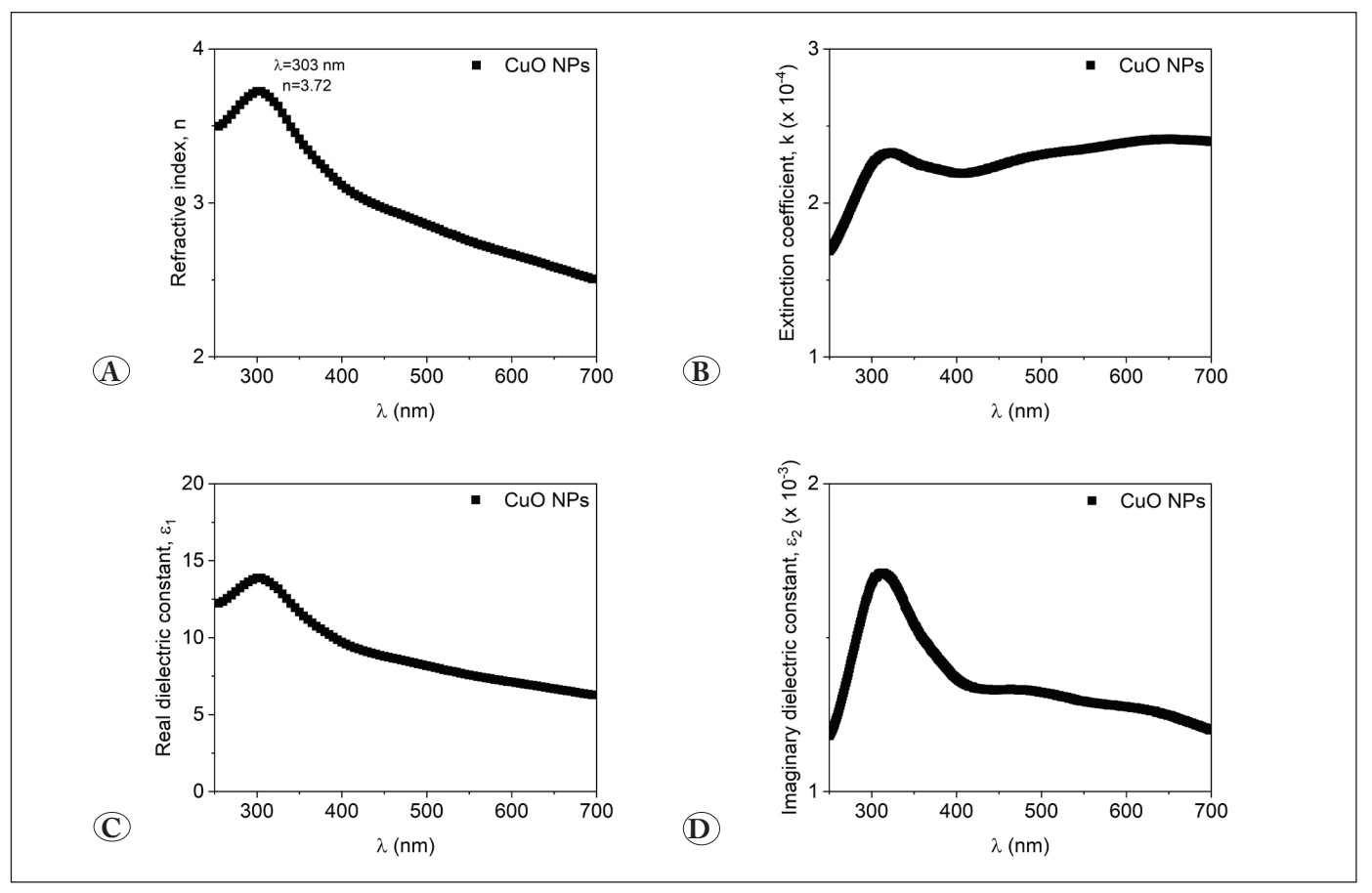


Figure 5. Dependence of the **A)** refractive index n, **B)** extinction coefficient k, **C)** real dielectric constant ε_1 , and **D)** imaginary dielectric constant ε_2 of CuO NPs on the wavelength.

NPs, interactions with 200 keV energy photons resulted in minimal radiation attenuation, with approximately 15% of the incident radiation being absorbed by the material. This low attenuation is attributed to the energy of the photons, which primarily interact with the CuO NPs via the photoelectric effect and, to a lesser extent, Compton scattering (Sayyed et al. 2025).

The energy deposition values obtained from the FLUKA simulations were found to be consistent with those derived from the Phy-X/PSD program for similar photon energies, confirming the accuracy of the simulation results (Figure 8).

The simulation representation of the energy storage capacity of CuO NP materials as a result of interactions with 200 keV and 900 keV photons is given in Figure 9. Figure 9 shows that the midpoint of the target is 29.2 keV/cm³/pp at 200 keV, 24.4 keV/cm³/pp at 300 keV, 18.1 keV/cm³/pp at 400 keV, 14.2 keV/cm³/pp at 500 keV, 14.1 keV/cm³/pp at 600 keV, 9.61 keV/cm³/pp at 700 keV, 8.37 keV/cm³/pp at 800 keV, and 7.39 keV/cm³/pp at 900 keV. These findings indicate that the center of the CuO NPs stores the maximum energy. There was a decrease in energy accumulation as one moved away from the center of the material.

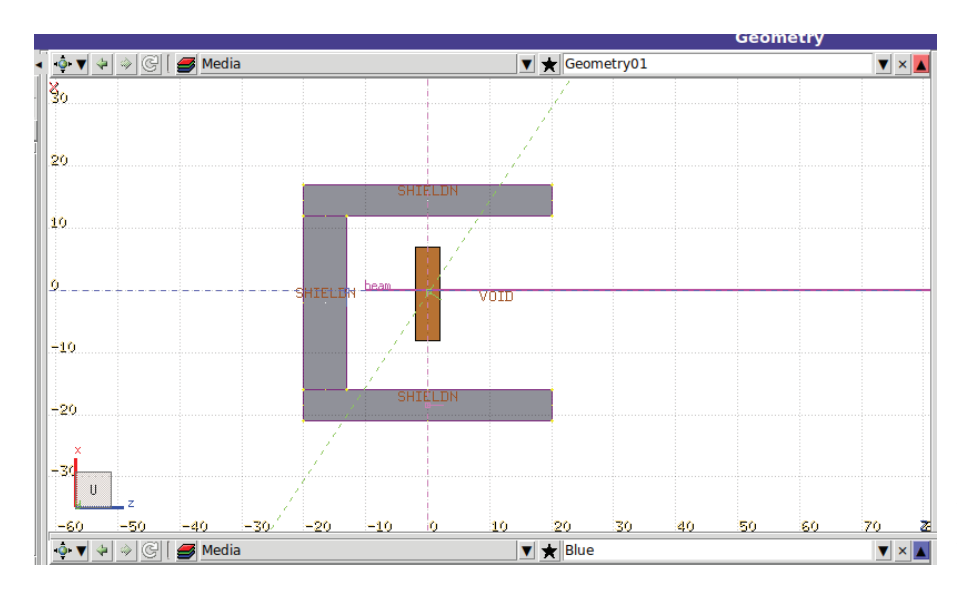


Figure 6. FLUKA simulation setup with a target sample.

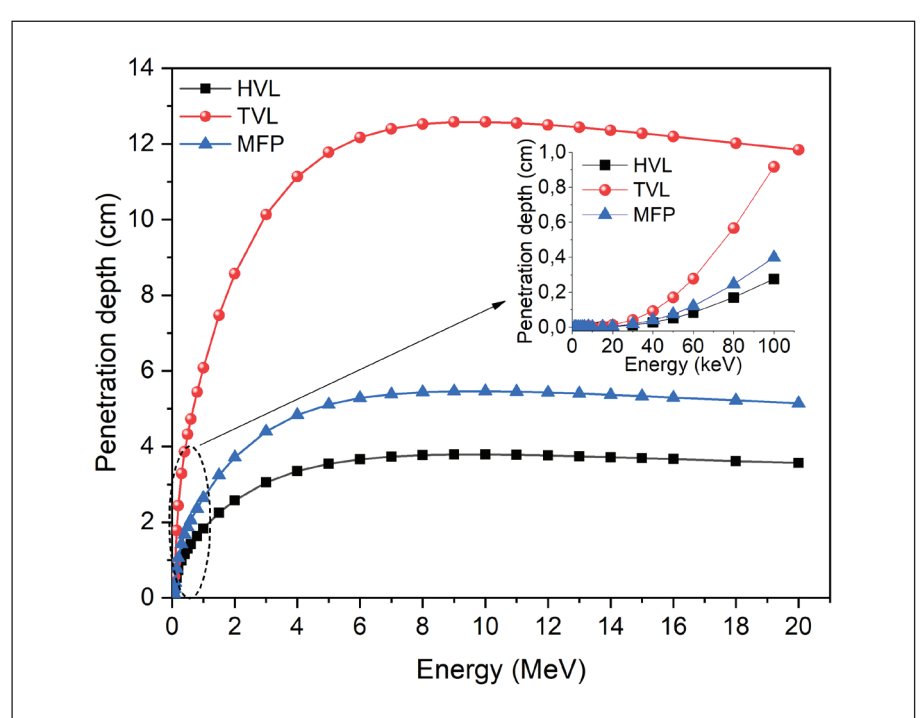


Figure 7. Comparison of the penetration depth values of the HVL, TVL and MFP (inset: 0.1–100 keV region).

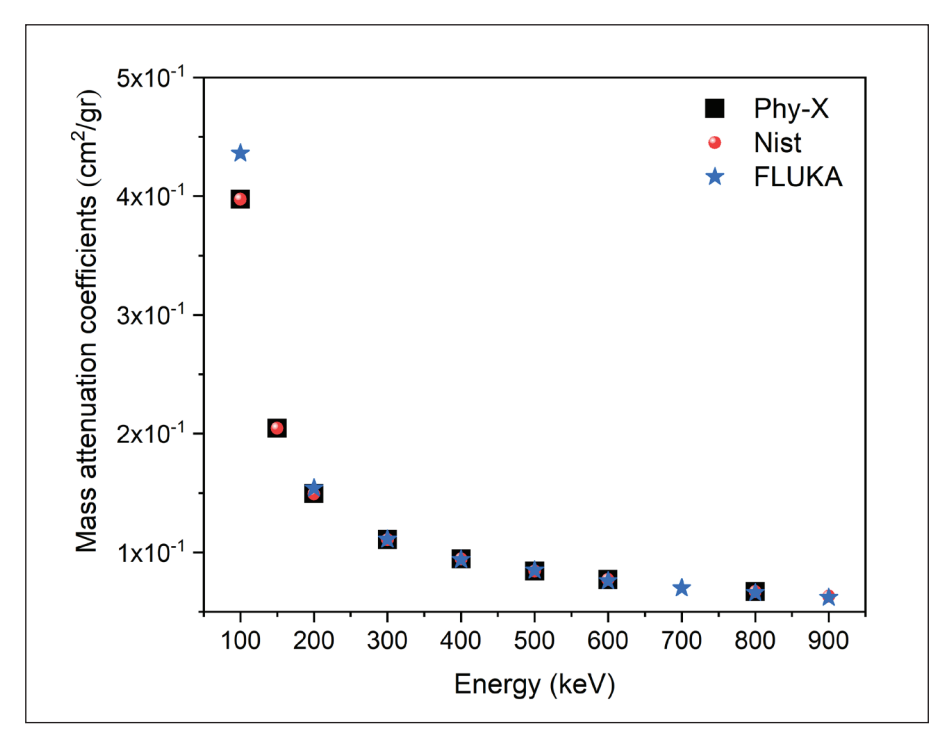


Figure 8. Mass attenuation coefficients (μ/ρ) obtained from Phy-X/PSD, NIST, and FLUKA for photon energies in the keV range.

In addition to energy deposition, the radiation absorption properties of the CuO NPs were evaluated via FLUKA and compared with the results obtained from the Phy-X/PSD and NIST programs. All three programs were used to model the interaction of photons with the material.

The results from NIST and Phy-X/PSD exhibited similar trends regarding energy absorption by the material. Both the NIST and Phy-X/PSD programs revealed that CuO NPs have the ability to absorb and attenuate radiation. The NIST, FLUKA, and Phy-X/PSD programs all revealed that there was no significant change in the mass attenuation coefficients between the 600 and 900 keV photon energies.

The study results demonstrate that the attenuation properties of CuO NPs vary with photon energy, which is consistent with the expected behavior of shielding materials. The mass attenuation coefficient decreases with increasing photon energy, highlighting the effectiveness of the material in attenuating low-to-moderate energy radiation (Sayyed et al. 2025). The high atomic number of copper contributes significantly to the absorption of photons, especially in the lower energy range. The CuO NPs show considerable potential for radiation shielding, particularly against low-to-moderate energy photons, as confirmed by the FLUKA simulation results. The material's HVL, TVL, and MFP values suggest that it performs efficiently in environments with low-energy photon sources, making it suitable for

specific medical and industrial applications. However, its effectiveness against high-energy gamma radiation is lower, indicating the need for further optimization in terms of density or thickness to improve performance in high-energy environments. For lower-energy photons (such as 100 keV), both FLUKA and Phy-X resulted in higher energy deposition and absorption near the material's center. In earlier studies, the influence of CuO on the linear attenuation coefficient (LAC) was investigated, and the results revealed a positive relationship between the CuO concentration and LAC value (Sayyed et al. 2025). These findings further support the conclusion that CuO materials are effective materials for radiation shielding and are suitable for applications in the nuclear, medical, and space industries.

4. Conclusion and Suggestions

The structural, morphological, optical, and radiation attenuation performance of the CuO nanoparticles was studied. The XRD results confirmed the presence of monoclinic CuO NP phases. The SEM images revealed that the material surface exhibited an agglomerated nanoparticle morphology, forming a porous flower-like structure. The refractive index, extinction coefficient, and real and imaginary parts of the dielectric constant were found. At a wavelength of 550 nm, the refractive index (n) and extinction coefficient (k) were determined to be 2.75 and 0.00024, respectively, corresponding to real and imaginary parts of the dielectric

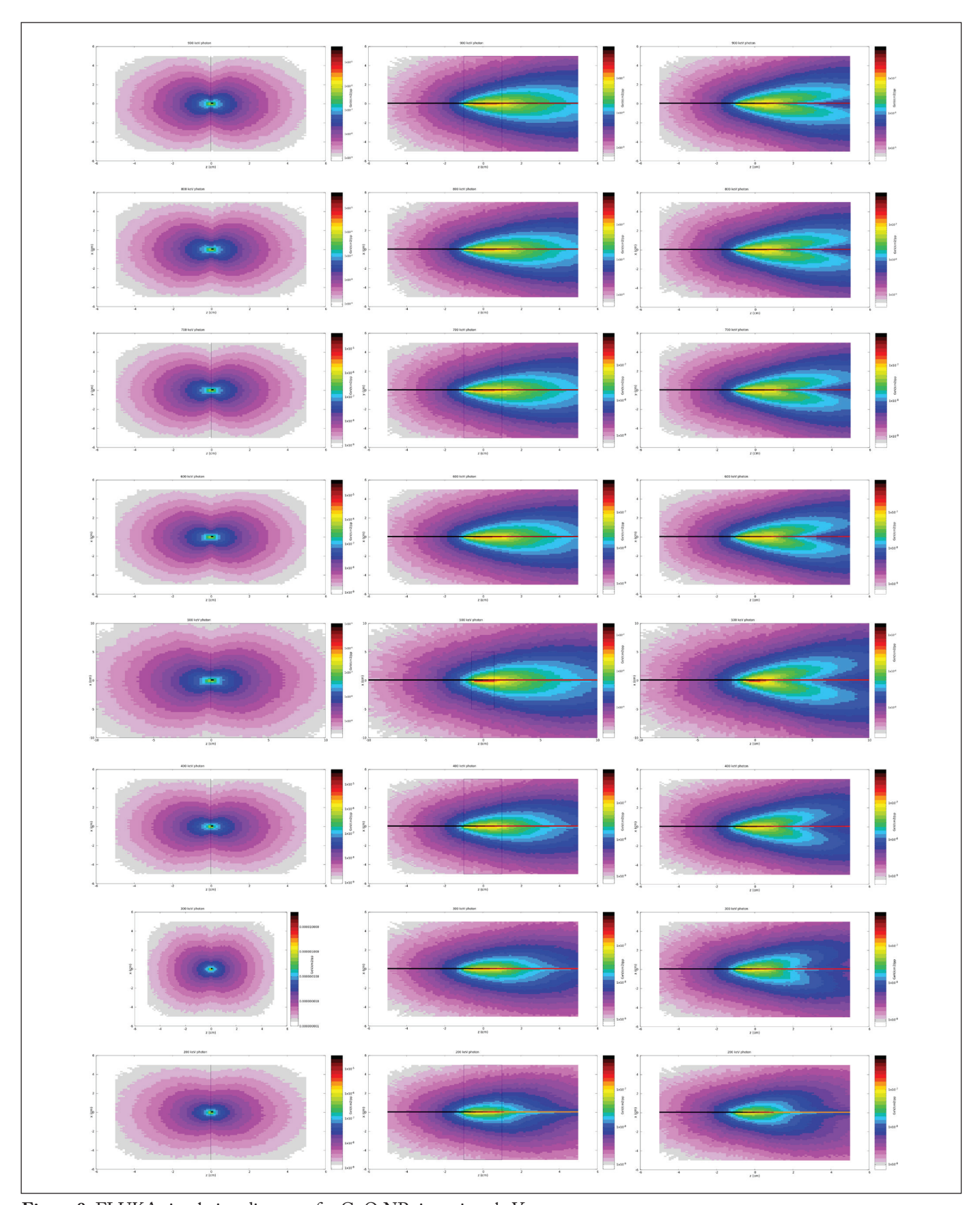


Figure 9. FLUKA simulation diagrams for CuO NPs in various keV energy ranges.

function (ϵ_1 and ϵ_2) as 7.570 and 0.0013. As a result, sharp absorption edges in the 500–650 nm wavelength region were observed, together with a calculated energy band gap of 2.88 eV. Additionally, this study demonstrated their radiation shielding capabilities. The half value layer (HVL), tenth value layer (TVL), and mean free path (MFP) were determined, and the results showed that at 100 keV, the HVL, TVL, and MFP were 0.27 cm, 0.91 cm, and 0.39 cm, respectively. This study revealed that although the nanoparticle synthesis processes are simple, CuO NPs have potential for use in radiation shielding and medical radiology applications.

Declaration of competing interest: The author declare that I have no competing interests.

Author contributions: Saniye Tekerek: planned and designed the study, gathered and analyzed data about the study, wrote the article by analyzing the study.

5. References

- Agar, O., Sayyed, MI., Akman, F., Tekin, HO., Kaçal, MR. 2019. An extensive investigation on gamma ray shielding features of Pd/Ag-based alloys. Nuclear Engineering and Technology, 51(3), 853-859. https://doi.org/10.1016/j.net.2018.12.014
- Ali, AM., Issa, SA., Ahmed, MR., Saddeek, YB., Zaid, MHM., Sayed, M., Somaily, H. H., Tekin, HO., Sidek, HAA., Matori, KA., Zakaly, HM. 2020. Promising applicable heterometallic Al2O3/PbO2 nanoparticles in shielding properties. Journal of Materials Research and Technology, 9(6), 13956-13962. https://doi.org/10.1016/j.jmrt.2020.09.125
- Alzahrani, JS., Alrowaili, ZA., Sriwunkum, C., Al-Buriahi, MS. 2024. Radiation and nuclear shielding performance of tellurite glass system containing Li₂O and MoO₃: XCOM and FLUKA Monte Carlo. Journal of Radiation Research and Applied Sciences, 17(2), 100923. https://doi.org/10.1016/j.jrras.2024.100923
- Amri, A., Hasan, K., Taha, H., Rahman, MM., Herman, S.,
 Awaltanova, E., Wantono, I., Kabir, H., Yin, CY., Ibrahim,
 K., Bahri, S., Frimayanti, N., Hossain, MA., Jiang, Z.
 T. 2019. Surface structural features and optical analysis of nanostructured Cu-oxide thin film coatings coated via the solgel dip coating method. Ceramics International, 45(10), 12888-12894. https://doi.org/10.1016/j.ceramint.2019.03.213
- Ballarini, F., Battistoni, G., Campanella, M., Carboni, M., Cerutti, F., Empl, A., Fassò, A., Ferrari, A., Gadioli, E., Garzelli, MV. 2006. The FLUKA code: an overview. In Journal of Physics: Conference Series, IOP Publishing, 41, 151–160. https://doi.org/10.1088/1742-6596/41/1/014

- Basith, NM., Vijaya, JJ., Kennedy, LJ., Bououdina, M. 2013. Structural, optical and room-temperature ferromagnetic properties of Fe-doped CuO nanostructures. Physica E: Low-dimensional Systems and Nanostructures, 53, 193-199. https://doi.org/10.1016/j.physe.2013.05.009
- Chen, Y., Zhang, L., Zhang, H., Zhong, K., Zhao, G., Chen, G., Lin Y, Chen S., Huang, Z. 2018. Band gap manipulation and physical properties of preferred orientation CuO thin films with nano wheatear array. Ceramics International, 44(1), 1134-1141. https://doi.org/10.1016/j.ceramint.2017.10.070
- Dridi, W., Alsulami, RA., Albarqi, MM., Alsufyani, SJ., Hosni, F. 2024. Radiation shielding features of Na2O–P2O5 glasses doped with MnO experimentally and using FLUKA and Phy-X. Journal of Radiation Research and Applied Sciences, 17(1), 100805. https://doi.org/10.1016/j.jrras.2023.100805
- El-Taher, A., Zakaly, HM., Allam, EA., El-Sharkawy, RM., Al Meshari, M., Soliman, A.M., ... Mahmoud, ME. 2025. Fluka and microshield simulation assessment of nuclear radiation attenuation by binary nanocomposites. Radiation Physics and Chemistry, 229, 112409. https://doi.org/10.1016/j.radphyschem.2024.112409
- Ferrari, A., Sala, PR., Fasso, A., Ranft, J. 2005. FLUKA: A Multi-Particle Transport Code. CERN-library, 55(99), 100. https://cds.cern.ch/record/898301
- Hubbell, JH. 1969. Photon Cross Sections, Attenuation Coefficients and Energy Absorption Coefficients from 10 keV to 100 GeV, Natl. Stand. Ref. Data Ser. 29.
- Hubbell, JH., Seltzer, SM. 2004. Cross section data for electron-positron pair production by photons: a status report. Nuclear Instruments and Methods in Physics Research Section B: Beam Interactions with Materials and Atoms, 213, 1-9. https://doi.org/10.1016/S0168-583X(03)01524-6
- Mansy, MS., Lasheen, YF., Breky, MM., Selim, Y. 2021. Experimental and theoretical investigation of Pb–Sb alloys as a gamma-radiation shielding material. Radiation Physics and Chemistry, 183, 109416. https://doi.org/10.1016/j.radphyschem.2021.109416
- Meulepas, JM., Hauptmann, M., Lubin, JH., Shuryak, I., Brenner, DJ. 2018. Is there unmeasured indication bias in radiation-related cancer risk estimates from studies of computed tomography. Radiat. Res., 189(2), 128-135. https:// doi.org/10.1667/RR14807.1
- Moss, TS., Burrell, GJ., Ellis, B. 1973. Semiconductor Optoelectronics. John Wiley & Sons, New York.
- Mullenders, L., Atkinson, M., Paretzke, H., Sabatier, L., Bouffler, S. 2009. Assessing cancer risks of low-dose radiation. Nat. Rev. Cancer., 9(8): 596–604. https://doi.org/10.1038/ nrc2677

- Nandhakumar, E., Priya, P., Selvakumar, P., Vaishnavi, E., Sasikumar, A., Senthilkumar, N. 2019. One step hydrothermal green approach of CuO/Ag nanocomposites: Analysis of structural, biological activities. Mater. Res. Express., 6(9): 0950g4. https://doi.org/10.1088/2053-1591/ab2eb9
- Nitta, R., Kubota, Y., Kishi, T., Matsushita, N. 2022. Fabrication of nanostructured CuO NPs with controllable optical band gaps using a mist spin spray technique at 90 °C. Thin Solid Films, 762: 139555. https://doi.org/10.1016/j.tsf.2022.139555
- Perkowitz, S. 1993. Optical Characterizations of Semiconductors: Infrared, Raman, and Photoluminescence Spectroscopy. Academic Press, San Diego.
- Rai, RS. 2024. Carbon fiber fabrics functionalized with monoclinic CuO nanostructures using seed-assisted hydrothermal growth treatment. Ceram. Int. 50(21): 44635–44647. https://doi. org/10.1016/j.ceramint.2024.08.311
- Rehman, SU., Khan, S., Iqbal, Z., Bilal, M., Alkhybari, E., Alhailiy, A., ... Alotaibi, S. 2025. Simulation of shielding parameters of Gd–Pb binary alloys using FLUKA code and Phy-x/PSD platform. Radiation Physics and Chemistry, 230, 112582. https://doi.org/10.1016/j.radphyschem.2025.112582
- Sagadevan, S., Pal, K., Chowdhury, ZZ. 2017. Fabrication of CuO nanoparticles for structural, optical and dielectric analysis using chemical precipitation method. J. Mater. Sci. Mater. Electron., 28(17): 12591–12597. https://doi.org/10.1007/ s10854-017-7083-3

- Sayyed, MI., Lakshminarayana, G., Dong, MG., Ersundu, MÇ., Ersundu, AE., Kityk, IV. 2018. Investigation on gamma and neutron radiation shielding parameters for BaO/SrO-Bi2O3-B2O3 glasses. Radiation Physics and Chemistry, 145, 26–33. https://doi.org/10.1016/j.radphyschem.2017.12.010
- Sayyed, MI., Rashad, M., Elsafi, M., Maghrbi, Y. 2025. The impact of CuO in modifying the radiation shielding performance of PbO–BaO–CaO–B2O3–CuO: An experimental approach. Radiation Physics and Chemistry, 226, 112271. https://doi.org/10.1016/j.radphyschem.2024.112271
- **Stokes, AR., Wilson, AJC. 1944.** The diffraction of X rays by distorted crystal aggregates-I. Proc. Phys. Soc., 56(3): 174.
- Şakar, E., Özpolat, ÖF., Alım, B., Sayyed, MI., Kurudirek, M. 2020. Phy-X/PSD: development of a user friendly online software for calculation of parameters relevant to radiation shielding and dosimetry. Radiation Physics and Chemistry, 166, 108496. https://doi.org/10.1016/j.radphyschem.2019.108496
- Tauc, J. 1974. Amorphous and Liquid Semiconductors. Plenum Press, New York.
- Wooten, F. 1972. Optical Properties of Solids. Academic Press, New York.